

4. Kaiser, M. K. & Hecht, H. Time-to-passage judgments in non-constant optical flow fields. *Percept. Psychophys.* **57**, 817–825 (1995).
5. Regan, D. & Beverley, K. I. Illusory motion in depth: aftereffect of adaptation to changing size. *Vision Res.* **18**, 209–212 (1978).
6. Regan, D. & Beverley, K. I. Binocular and monocular stimuli for motion in depth: changing-disparity and changing-size feed the same motion-in-depth stage. *Vision Res.* **19**, 1331–1340 (1979).
7. Morrone, M. C., Burr, D. C., Di Pietro, S. & Stefanelli, M. Cardinal directions for visual optic flow. *Curr. Biol.* **9**, 763–766 (1999).
8. Orban, G. A. *et al.* First-order analysis of optical flow in monkey brain. *Proc. Natl. Acad. Sci. USA* **89**, 2595–2599 (1992).
9. Duffy, C. J. & Wurtz, R. H. Sensitivity of MST neurons to optic flow stimuli: I. a continuum of response selectivity to large-field stimuli. *J. Neurophysiol.* **65**, 1329–1345 (1991).
10. Gibson, J. J. *The Perception of the Visual World* (Houghton Mifflin, Boston, 1950).
11. Warren, W. H., Morris, M. W. & Kalish, M. L. Perception of translational heading from optical flow. *J. Exp. Psychol. Hum. Percept. Perform.* **14**, 646–660 (1988).
12. Warren, W. H., Blackwell, A. W., Kurtz, K. J., Hatsopoulos, N. G. & Kalish, M. L. On the sufficiency of the velocity field for perception of heading. *Biol. Cybern.* **65**, 311–320 (1991).
13. Perrone, J. A. Model for the computation of self-motion in biological systems. *J. Opt. Soc. Am. A* **9**, 177–194 (1992).
14. Crowell, J. A. & Banks, M. S. Perceiving heading with different retinal regions and types of optic flow. *Percept. Psychophys.* **53**, 325–337 (1993).
15. Beverley, K. I. & Regan, D. Texture changes versus size changes as stimuli for motion in depth. *Vision Res.* **23**, 1387–1400 (1983).
16. Anstis, S. M. The perception of apparent movement. *Phil. Trans. R. Soc. Lond. B* **290**, 153–168 (1980).
17. Cavanagh, P. & Mather, G. Motion: the long and short of it. *Spatial Vis.* **4**, 103–129 (1989).
18. Blake, R. & Hirsh, E. Another means for measuring the motion aftereffect. *Vision Res.* **33**, 1589–1592 (1993).
19. Perrone, J. A. Anisotropic responses to motion toward and away from the eye. *Percept. Psychophys.* **39**, 1–8 (1986).
20. Tyler, C. & Sutter, E. Depth from spatial frequency difference: An old kind of stereopsis? *Vision Res.* **19**, 859–865 (1979).
21. Tian, R. & Rauschecker, J. P. Processing of frequency-modulated sounds in the cat's posterior auditory field. *J. Neurophysiol.* **79**, 2629–2642 (1998).
22. Watson, A. B. & Pelli, D. G. Quest: A Bayesian adaptive psychophysical method. *Percept. Psychophys.* **33**, 113–120 (1983).
23. Kendall, M. K. & Stuart, A. *The Advanced Theory of Statistics: Vol. 3. Design, Analysis, and Time Series* (Hafner, New York, 1966).

#### Acknowledgements

This work was begun when all three authors were at the University of Pennsylvania. P.S. was supported by a training grant from the NEI at the University of Pennsylvania and by a research grant from the NIH at the University of Minnesota; E.S. was supported by the National Science Foundation and the Alfred P. Sloan Foundation; and D.K. was supported by a research grant from the NIH.

Correspondence and requests for materials should be addressed to P.S. (e-mail: schrater@eye.psych.umn.edu).

## The motor side of depth vision

**Kai Schreiber\***†, **J. Douglas Crawford†‡**, **Michael Fetter§**  
**& Douglas Tweed\*†‡**

\* Departments of Physiology and Medicine, University of Toronto,  
 1 King's College Circle, M5S 1A8 Toronto, Canada

† Canadian Institutes of Health Research, Group for Action and Perception  
 ‡ Centre for Vision Research, York University, 4700 Keele Street, M3J 1P3 Toronto,  
 Canada

§ Department of Neurology, University Hospital Tübingen,  
 Hoppe-Seyler-Straße 3, 72072 Tübingen, Germany

To achieve stereoscopic vision, the brain must search for corresponding image features on the two retinas<sup>1</sup>. As long as the eyes stay still, corresponding features are confined to narrow bands called epipolar lines<sup>2,3</sup>. But when the eyes change position, the epipolar lines migrate on the retinas<sup>4–6</sup>. To find the matching features, the brain must either search different retinal bands depending on current eye position, or search retina-fixed zones that are large enough to cover all usual locations of the epipolar lines. Here we show, using a new type of stereogram in which the depth image vanishes at certain gaze elevations, that the search zones are retina-fixed. This being the case, motor control acquires a crucial function in depth vision: we show that the eyes twist

about their lines of sight in a way that reduces the motion of the epipolar lines, allowing stereopsis to get by with smaller search zones and thereby lightening its computational load.

Eye motion shifts the epipolar lines—the retinal bands where corresponding image features, or stereo matches, project in the two eyes. In the simulation shown in Fig. 1, if the small open circles represent point images cast onto the right retina, and the eyes are converged 30° while looking level, then the corresponding images on the left retina must lie somewhere along the thick lines. When the eyes look 30° down, still converged 30°, the images on the left retina must lie on the thin lines in Fig. 1. When the eyes look 30° up, the images lie on the dashed lines. If the brain searches the wrong lines for stereo matches, it will not find them and stereopsis will fail.

This is a fundamental problem facing any creature that wants both stereopsis and mobile eyes, and there are just two possible solutions. Either the matching algorithm searches different retinal bands depending on current eye position, or it searches eye-fixed zones large enough to encompass all possible locations of the epipolar lines in all usual eye configurations (outlined regions in Fig. 1). Most theories of stereopsis assume that the brain searches narrow bands, so as to reduce its computational load. We used visual stimuli like those in Fig. 2 to show that in fact the brain uses large, eye-fixed zones.

Discs a1 and a2 in Fig. 2 form a cyclorotated stereogram (b1 and b2 form another, interleaved to save space on the page). Disc a1, to be viewed by the right eye, is rotated 2° counterclockwise, and a2 is rotated 2° clockwise, for a total of 4° incyclorotation. When humans converge and look down, our eyes incyclorotate, with the upper poles of both eyes rotating medially<sup>5,7,8</sup>. When we converge and look up, our eyes excyclorotate. If stereo matching adjusts its search to correct for eye position, this cyclorotation should make no difference to vision; but if the matching algorithm does not correct for eye position, we should see incyclorotated stereograms better when we look down, and excyclorotated stereograms better when we look up. If you fuse the stereograms of Fig. 2 as instructed in the figure legend, you should see the stereoscopic images only on downgaze.

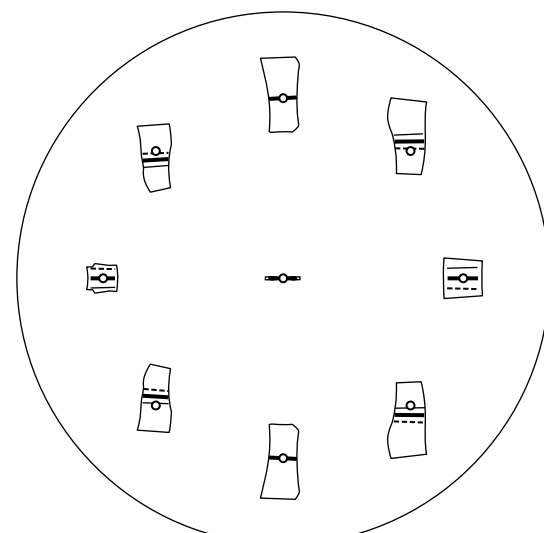


**Figure 1** Epipolar lines vary with eye position. The nine open circles are images of nine objects projected onto the right retina, one foveal and the rest 15° eccentric (the perimeter circle marks 22.5° from the fovea). Projections of these same objects onto the left retina must lie somewhere on the thick line segments—pieces of epipolar lines—when the eyes converge 30° and look level. They lie on the dashed lines when the eyes look up 30° and on the thin lines when they look down 30°, always with 30° of convergence. Outlines mark the entire range of motion of the epipolar segments when the eyes also move ± 20° horizontally. Eye motion in this simulation is a realistic combination of Listing's law and L2 (see Methods).

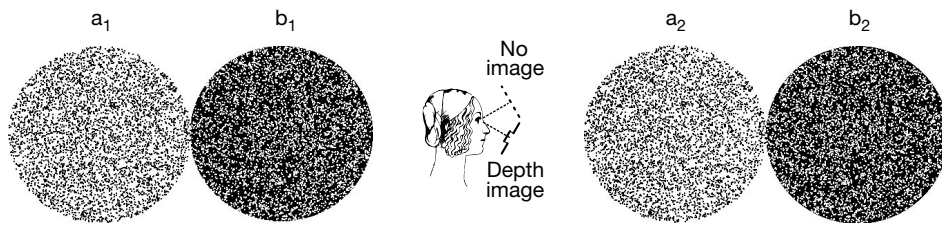


**Figure 2** Cyclorotated stereograms are visible only in certain eye positions. Cross-fuse discs a1 and a2 from 30 cm away, depressing your gaze as far as possible and holding the paper orthogonal to the plane of your sight lines (not parallel to your face). You should see a depth image (a pointer, like a tapering clock hand, pointing up and right) in this position, but not when you do the same on upgaze. Flipping the page upside-down yields a

We tested five normal subjects, all of whom showed this positional stereoblindness. When one typical subject viewed stereograms while converged 30° and looking 30° down, he could reliably see depth—that is he could identify the disparity-defined image at least 50% of the time—in stereograms that were incyclorotated as much as 10.1° (Fig. 3). Looking up, his threshold was just 3.0° of incyclorotation. So a stereogram with, for example, 7° of incyclorotation was visible on downgaze but not on upgaze. For excyclorotation the subject's thresholds were better when he looked up, so that a stereogram with 7° of excyclorotation was visible on upgaze but not on downgaze. Thresholds varied between subjects, but all five showed the pattern of positional stereoblindness (Fig. 4) that one would expect if the matching algorithm were receiving no information about eye position.

Eye-position measurements quantitatively confirmed this idea. In all five subjects, we plotted cyclorotation thresholds versus cyclovergence measured by the nonius method<sup>4,9</sup> (Fig. 4). If search zones are perfectly fixed to the retinas, the slope of these lines will be 1 (parallel to the dashed line in the figure), meaning that the cyclorotation thresholds rotate exactly as far as the eyes. On average, the slope was 1.06. We conclude that stereoptic search zones are essentially eye-fixed.

This finding suggests that eye control might be an important part of stereopsis. An optimized motor program could coordinate the eyes in a way that minimizes the motion of the epipolar lines and therefore allows stereopsis to get by with the smallest possible search zones, lightening the computational load. What is the optimal pattern of eye coordination? Horizontal and vertical motions of both eyes are determined by the visual fixation target, but cyclovergence is free: both eyes can turn about their lines of sight without

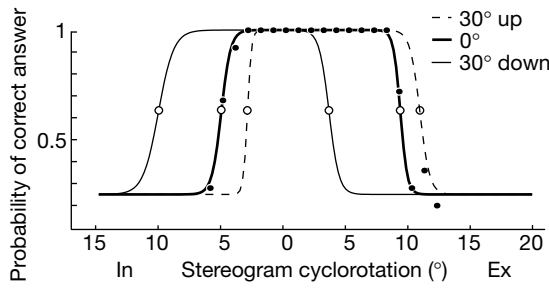


**Figure 3** Stereopsis depends on gaze elevation. For this typical subject, black dots show the fraction of images that were correctly perceived or guessed—there was always a 25% chance of guessing which of the four possible disparity-defined images was present—as a function of the cyclorotation of the stereograms, when the subject converged 30° and looked level. Fitted curves plot performance at three gaze elevations. Open circles mark perception thresholds, that is, angles at which stereograms were reported correctly 62.5% of the time; this is the performance expected when the subject perceives the image 50% of the time and guesses correctly on a quarter of the remaining trials.

stereogram visible only on upgaze. If the image never disappears, your search zones are too large for this stereogram; try fusing discs b1 and b2, whose cyclorotation is greater (10°). If no image appears even on downgaze, your search zones are too small; try fusing a1 and a2 upside-down.

breaking fixation. Our simulations showed that cyclovergence—equal cyclorotation of the two eyes—makes little difference to stereopsis, but cyclovergence matters.

We considered how cyclovergence is controlled. Does it respond to visual stimuli? Do the eyes excycloverge, for example, when they see an excyclorotated stereogram? We used search coils to measure eye motion in six subjects viewing cyclorotated stereograms, and found that, on average, cyclovergence varied only 0.07° (range 0.02–0.16°) for every degree of stimulus cyclorotation. Larger or moving stimuli evoke stronger eye rotations<sup>10–13</sup>, but even then visually driven cyclovergence is superimposed on a blind, default pattern of eye control<sup>10</sup>.

The normal pattern of eye control when viewing distant objects is Listing's law<sup>14,15</sup>, which states that each eye's cyclorotation is proportional to the product of its horizontal and vertical angles in radians,  $C = -HV/2$  (see Methods). By this formula, Listing's law calls for a cyclovergence range of 15.7° in our experiment, from 7.85° excyclorotation on upgaze to 7.85° incyclorotation on downgaze. But in fact, the ranges of our subjects averaged just 6.8° (Fig. 4); that is, our subjects, like those of other studies<sup>7,8,16–19</sup>, violated Listing's law on near gaze, reducing their cyclovergence<sup>5</sup>.

Obeying Listing's law brings many functional advantages, improving motor efficiency and simplifying monocular visual processing<sup>5,14,20,21</sup>. So there must be some even greater functional advantage, incompatible with Listing's law, to make the brain violate

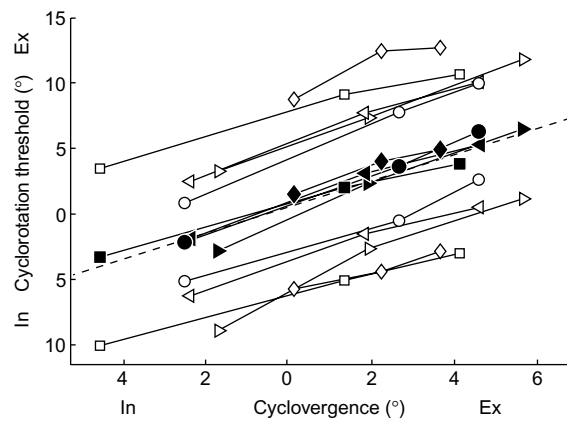


**Figure 4** Perception thresholds depend on gaze elevation and cyclovergence. Open symbols at top and bottom mark excyclorotation and incyclorotation thresholds for five subjects. Filled symbols lie halfway between the two thresholds, at the midpoint of the visible range. Thresholds for all five subjects varied significantly with gaze elevation, shifting toward incyclorotation on downgaze (leftmost symbol in each string of three) and toward excyclorotation on upgaze (rightmost symbol in each string of three);  $F_{2,8} = 33.40$ ,  $P < 0.001$  for incyclorotation thresholds,  $F_{2,8} = 51.95$ ,  $P < 0.001$  for excyclorotation. These plots of perception thresholds versus cyclovergence show an average slope of 1.06, very close to slope of 1 (the dashed line) predicted if stereo matching receives no information about eye position.

it so markedly on near gaze<sup>5,8</sup>. The advantage, we suggest, is that reducing cyclovergence restricts the motion of the epipolar lines, permitting stereo matching to function with smaller search zones. Still smaller zones would be possible if cyclovergence were eliminated entirely, and a further slight improvement would accrue if cycloversion were also avoided; however, the brain rejects these motor patterns, presumably because they stray too far from Listing's law. Thus, eye control strikes a balance between the motor and monocular advantages of Listing's law and the optimization of stereoptic search.

We computed the smallest search zones that would permit stereopsis, given different patterns of eye control. Listing's law yields the black zones in Fig. 5. Eliminating cyclovergence allows stereopsis to proceed with much smaller zones—the white regions. Such plots show how the layout of an optimized visual system depends on the pattern of eye motion. As human eye control lies between these two patterns, our search zones should show an intermediate arrangement, closer to the white. (The zones may be slightly taller than predicted here because we consider only the effects of eye motion, whereas there may be other reasons for vertical search<sup>22</sup>.) As Fig. 5 shows, search zones should be flatter along the retina's horizontal meridian, taller eccentrically and smaller temporally, whereas on oblique meridians they should be vertically displaced relative to the corresponding dot on the other retina. These predictions can be tested perceptually and electrophysiologically, by plotting receptive fields of groups of visual neurons. For example, an optimal system would tolerate vertical disparities of about  $0.1^\circ$  within  $1^\circ$  of the foveal centre and  $0.7^\circ$  at  $3^\circ$  eccentricity; these predictions are consistent with the available data<sup>4,23,24</sup>, and explain why vertical tolerance increases rapidly with retinal eccentricity.

Stereopsis, then, is partly a motor process. The stereo-matching algorithm does not know where it is looking, and therefore does not move its search zones on the retinas when the eyes move; instead, it uses eye-fixed search zones and relies on ocular coordination to keep corresponding images within these bounds. A motor program twists the eyes about their lines of sight in a way that reduces the motion of the epipolar lines, allowing stereopsis to operate with smaller search zones. □

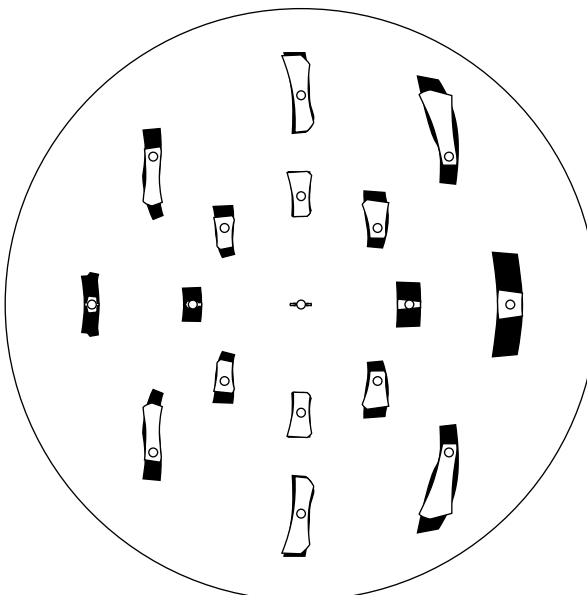


**Figure 5** Optimal stereoptic search zones when the eyes obey Listing's law (black areas) and when they move without cyclovergence (white areas) in a pattern called L2 (see Methods). Rings of dots are  $15^\circ$  and  $30^\circ$  from the fovea, the perimeter circle is at  $45^\circ$ . Simulated eye positions ranged from  $-20^\circ$  to  $20^\circ$  horizontal version,  $-30^\circ$  to  $30^\circ$  vertical version and  $0^\circ$  to  $30^\circ$  vergence.

## Methods

### Perceptual experiments

Subjects viewed three series of 200 stereograms each at eye level and  $30^\circ$  above and below. Stereograms appeared on a notebook-computer screen 35 cm away in darkness, spaced so that cross-fusion required  $30^\circ$  of vergence; at each of the three gaze elevations, the screen was rotated so that it was orthogonal to the visual plane. Each disc of each stereogram spanned  $1^\circ$  and comprised 2,000 white dots on a black screen. Each stereogram contained a disparity-defined shape—a pointer, like a clock hand, pointing in one of four oblique directions, presented in random order.

Stereograms were flashed for 200 ms; subjects then chose the direction in which they thought the clock hand was pointing. An interactive program varied the cyclorotation angles of the stereograms depending on the correctness of previous answers, mapping out the threshold ranges. Because subjects viewed the stereograms cross-eyed, their lines of sight hit the flat computer screen at a  $15^\circ$  slant. To eliminate the optical effects of this slant, we warped the random-dot patterns on the screen in a precise way so that each retinal projection was of a disc seen face-on, without slant-induced disparities, cyclorotated about the line of sight. But as slants are present in real life when one views near objects, we also performed the experiments without the de-slanting procedure.

The results were identical, all five subjects showing the same positional stereoblindness; in this version of the experiment, the average slope of the relation between perception thresholds and cyclovergence was 1.02, almost equal to the value of 1.06 in Fig. 4. In these with-slant experiments, we presented the stereograms for 8 s rather than 200 ms, to show that the positional stereoblindness also occurs with prolonged viewing. To show that the effect is not specific to judgements of orientation, we used 20 disparity-defined shapes, such as discs, squares or triangles, instead of a clock hand.

### Eye position

Eye positions are expressed in Helmholz angles<sup>5,8,14</sup>, with positive directions right, up and clockwise (other coordinate systems can mislead in vision studies because they obscure the relation between eye position and retinal correspondence; for example, when eye motion is expressed using quaternions or rotation vectors, converged eyes incycloverge on upgaze<sup>5,7,16</sup>, which makes it seem odd that excyclorotated stereograms are seen better). The best way of measuring Helmholz cyclovergence is the torsional nonius method<sup>4,9</sup>, but this does not allow the recording of eye position while stereograms are viewed. In six subjects, therefore, we also measured the 3D positions of both eyes using scleral search coils<sup>25,26</sup>.

### Simulations

To compute the white search zones in Fig. 5, we let the eyes move in a pattern known as L2 (ref. 5), in which  $C_R = -H_R V/2 - DV/4 = C_L = -H_L V/2 + DV/4$ ,  $C$  and  $H$  being the cyclorotation and horizontal angles of the right (R) and left (L) eyes,  $V$  their common vertical angle and  $D = H_L - H_R$  the vergence angle. Fig. 1 uses a motion pattern intermediate between L2 and Listing's law<sup>5,7</sup> with  $C_R = -H_R V/2 - 0.15DV$ ,  $C_L = -H_L V/2 + 0.15DV$ . In both figures the horizontal sizes of the search zones, and to a much lesser extent their heights, depend on the thickness of the stereo-matchable region around the 2D horopter<sup>25</sup>; we assume a thickness of  $\pm 3\%$  of the distance from the horopter to the eye because this value, in agreement with experimental data on quantitative stereopsis<sup>4</sup>, implies that subjects should detect horizontal disparities of up to about  $1^\circ$  at the fovea.

We also did simulations using much thicker stereo-matchable regions, up to  $\pm 50\%$  of the distance to the eye (with a matchable region this thick, the system would be able to detect disparities of up to  $32^\circ$  at the fovea). The search zones were then much larger, and the per cent reductions achieved by L2 compared to Listing's law were still considerable (for example, about 45% reduction for  $\pm 3\%$  thickness, 40% for  $\pm 20\%$ , 20% for  $\pm 50\%$ ). In Figs 1 and 5, the simulations use 'geometric' horopters; that is, they omit the Hering–Hillebrand deviation and the  $1^\circ$  declinations of corresponding near-vertical meridians<sup>5,15</sup>. Incorporating these small adjustments makes no significant difference to the simulations: L2 still shrinks the search zones by about the same amount.

Received 19 December 2000; accepted 29 January 2001.

1. Julesz, B. Binocular depth perception of computer-generated patterns. *Bell. Syst. Tech. J.* **39**, 1152–1162 (1960).
2. Ogle, K. *Researches in Binocular Vision* (Saunders, Philadelphia, 1950).
3. Rogers, B. J. & Bradshaw, M. F. Does the visual system use the epipolar constraint for matching binocular images? *Invest. Ophthalmol. Vis. Sci.* **37** (Suppl.), 31–25 (1996).
4. Stevenson S. B. & Schor, C. M. Human stereo matching is not restricted to epipolar lines. *Vision Res.* **37**, 2717–2723 (1997).
5. Tweed, D. Visual-motor optimization in binocular control. *Vision Res.* **37**, 1939–1951 (1997).
6. Gårding, J., Porrill, J., Mayhew, J. E. W. & Frisby, J. P. Stereopsis, vertical disparity and relief transformations. *Vision Res.* **35**, 703–722 (1995).
7. Mok, D., Ro, A., Cadena, W., Crawford, J. D. & Vilis, T. Rotation of Listing's plane during vergence. *Vision Res.* **32**, 2055–2064 (1992).
8. Van Rijn, L. J. & Van den Berg, A. V. Binocular eye orientation during fixations: Listing's law extended to include eye vergence. *Vision Res.* **33**, 691–708 (1993).
9. Howard, I. P., Ohmi, M. & Sun, L. Cyclovergence: a comparison of objective and psychophysical measurements. *Exp. Brain Res.* **97**, 349–355 (1993).
10. Hooge, I. Th. C. & van den Berg, A. V. Visually evoked cyclovergence and extended Listing's law. *J. Neurophysiol.* **83**, 2757–2775 (2000).
11. Crone, R. A. & Everhard-Halm, Y. Optically induced eye torsion. *Albrecht v. Graefes Arch. klin. exp. Ophthalm.* **195**, 231–239 (1975).
12. Hooton, K., Myers, E., Worrall, R. & Stark, L. Cyclovergence: The motor response to cyclodisparity. *Albrecht v. Graefes Arch. klin. exp. Ophthalm.* **210**, 65–68 (1979).

13. Kertesz, A. E., Sullivan, M. J. The effect of stimulus size on human cyclofusional response. *Vision Res.* **18**, 567–571 (1978).
14. Carpenter, R. H. S. *The Movements of the Eyes* (Pion, London, 1988).
15. Helmholz, H. von. *Handbuch der Physiologischen Optik* (Voss, Hamburg, 1867).
16. Minkin A. W. H. & Van Gisbergen, J. A. M. A three-dimensional analysis of vergence movements at various levels of elevation. *Exp. Brain Res.* **101**, 331–345 (1994).
17. Allen, M. J. The dependence of cyclophoria on convergence, elevation and the system of axes. *Am. J. Optom.* **31**, 297–307 (1954).
18. Kapoula, Z., Bernotas, M. & Haslwanter, T. Listing's plane rotation with convergence: role of disparity, accommodation, and depth perception. *Exp. Brain Res.* **126**, 175–186 (1999).
19. Steffen, H., Walker, M. F. & Zee, D. S. Rotation of Listing's plane with convergence: independence from eye position. *Invest. Ophthalmol. Vis. Sci.* **41**, 715–721 (2000).
20. Hepp, K. On Listing's law. *Commun. Math. Phys.* **132**, 285–292 (1995).
21. Hepp, K. Theoretical explanations of Listing's law and their implication for binocular vision. *Vision Res.* **35**, 3237–3241 (1995).
22. Farrell, B. Two-dimensional matches from one-dimensional stimulus components in human stereopsis. *Nature* **395**, 689–693 (1998).
23. Nielsen, K. R. & Poggio, T. Vertical image registration in stereopsis. *Vision Res.* **24**, 1133–1140 (1984).
24. Prazdny, K. Vertical disparity tolerance in random-dot stereograms. *Bull. Psychonom. Soc.* **23**, 413–414 (1985).
25. Robinson, D. A. A method of measuring eye movement using a scleral search coil in a magnetic field. *IEEE Trans. Biomed. Eng.* **10**, 137–145 (1963).
26. Tweed, D., Cadera, W. & Vilis, T. Computing three-dimensional eye position quaternions and eye velocity from search coil signals. *Vision Res.* **30**, 97–110 (1990).

## Acknowledgements

We thank D. Henriques, I. Howard, E. Klier, P. Nguyen, J. Sharpe, H. Wang, A. Wong and J. Zacher for help with experiments; and K. Beykirch, P. Hallett, C. Hawkins, D. Henriques, H. Misslisch, M. Niemeier and T. Vilis for comments on the manuscript. This study was supported by the Canadian Institutes for Health Research and the Deutsche Forschungsgemeinschaft. D.C. is a CIHR Scholar and D.T. a CIHR Scientist.

Correspondence and requests for materials should be addressed to D.T.  
(e-mail: douglas.tweed@utoronto.ca).

## Leptin-regulated endocannabinoids are involved in maintaining food intake

**Vincenzo Di Marzo\***, **Sravan K. Goparaju†**, **Lei Wang†‡**, **Jie Liu†‡**, **Sándor Bátkai†‡**, **Zoltán Járai†**, **Filomena Fezza†**, **Grant I. Miura§**, **Richard D. Palmiter§**, **Takayuki Sugiura||** & **George Kunos†‡**

\* Endocannabinoid Research Group, Istituto per la Chimica di Molecole di Interesse Biologico, CNR, 80072, Arco Felice, Naples, Italy

† Department of Pharmacology and Toxicology, Medical College of Virginia, Virginia Commonwealth University, Richmond, Virginia 23298, USA

§ Howard Hughes Medical Institute and Department of Biochemistry, University of Washington, Seattle, Washington 98195, USA

|| Faculty of Pharmaceutical Sciences, Teikyo University, Sagamiko, Kanagawa, 199-0195, Japan

Leptin is the primary signal through which the hypothalamus senses nutritional state and modulates food intake and energy balance<sup>1</sup>. Leptin reduces food intake by upregulating anorexigenic (appetite-reducing) neuropeptides, such as  $\alpha$ -melanocyte-stimulating hormone<sup>2,3</sup>, and downregulating orexigenic (appetite-stimulating) factors, primarily neuropeptide Y<sup>4</sup>. Genetic defects in anorexigenic signalling, such as mutations in the melanocortin-4 (ref. 5) or leptin receptors<sup>6</sup>, cause obesity. However, alternative orexigenic pathways maintain food intake in mice deficient in neuropeptide Y<sup>7</sup>. CB1 cannabinoid receptors<sup>8</sup> and the endocannabinoids anandamide and 2-arachidonoyl glycerol are present in the hypothalamus<sup>9</sup>, and marijuana<sup>10</sup> and anandamide<sup>11,12</sup> stimulate food intake. Here we show that following temporary food restriction, CB1 receptor knockout mice eat

less than their wild-type littermates, and the CB1 antagonist SR141716A reduces food intake in wild-type but not knockout mice. Furthermore, defective leptin signalling is associated with elevated hypothalamic, but not cerebellar, levels of endocannabinoids in obese *db/db* and *ob/ob* mice and Zucker rats. Acute leptin treatment of normal rats and *ob/ob* mice reduces anandamide and 2-arachidonoyl glycerol in the hypothalamus. These findings indicate that endocannabinoids in the hypothalamus may tonically activate CB1 receptors to maintain food intake and form part of the neural circuitry regulated by leptin.

CB1<sup>-/-</sup> and CB1<sup>+/+</sup> mice were made as described previously<sup>13,14</sup> and were maintained on a reverse light/dark cycle for measurement of food intake. After 18 h of fasting, the animals received a single intraperitoneal injection of vehicle or drug 10 min before the beginning of the dark cycle, and food intake was measured for the indicated period of time. After vehicle treatment, food intake was significantly lower in CB1<sup>-/-</sup> than in CB1<sup>+/+</sup> mice. When CB1<sup>+/+</sup> mice were treated with 3  $\mu\text{g g}^{-1}$  of the selective CB1 receptor antagonist SR141716A (ref. 15), food intake was significantly reduced to the same level as in vehicle-treated CB1<sup>-/-</sup> mice, whereas in CB1<sup>-/-</sup> mice SR141716A did not affect food intake (Fig. 1). These results indicate that endogenous cannabinoids acting at CB1 receptors may be involved in maintaining food intake in mice made hyperphagic by brief food deprivation.

As leptin is known to downregulate the expression in the hypothalamus of orexigenic peptides such as neuropeptide Y (NPY)<sup>4</sup>, orexins<sup>16</sup> and melanin concentrating hormone<sup>17</sup>, we investigated whether it may similarly regulate hypothalamic endocannabinoids. A single intravenous injection of 125 or 250  $\mu\text{g}$  of recombinant mouse leptin into normal Sprague–Dawley rats resulted in around 40–50% reductions in the hypothalamic levels of both anandamide and 2-arachidonoyl glycerol (2-AG) within 30 min, compared with levels in vehicle-treated controls (Fig. 2). By contrast, defective leptin signalling in obese Zucker rats was associated with elevated 2-AG levels in the hypothalamus compared with non-obese controls. The hypothalamic levels of anandamide and palmitoyl ethanolamide (PEA) were not significantly different in Zucker rats and their controls (Fig. 3a). In young (6–8-week-old) obese *db/db* mice with defective leptin receptors, hypothalamic levels of both 2-AG and anandamide were higher than in their

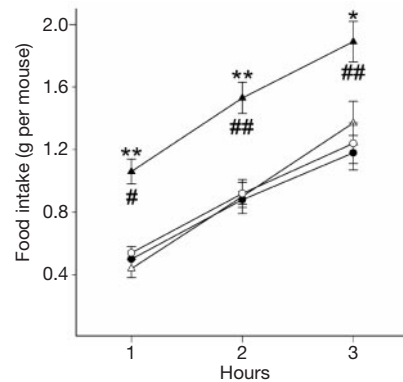


**Figure 1** Food intake in CB1<sup>-/-</sup> mice and their CB1<sup>+/+</sup> littermates in the absence and presence of the CB1 receptor antagonist SR141716A. Cumulative food intake was measured in 18-h food-restricted CB1<sup>-/-</sup> (circles) and CB1<sup>+/+</sup> mice (triangles). The animals received a single intraperitoneal injection of vehicle (filled symbols) or 3  $\mu\text{g g}^{-1}$  SR141716A (open symbols) 10 min before the start of the testing period. Means  $\pm$  s.e.,  $n = 9$  CB1<sup>+/+</sup> and 5 CB1<sup>-/-</sup> mice. Significance of difference from corresponding values in the presence of SR141716A in the same group of animals (\* $P < 0.05$ , \*\* $P < 0.01$ ), or from corresponding values in vehicle-treated CB1<sup>-/-</sup> mice (# $P < 0.05$ , ## $P < 0.01$ ) calculated by analysis of variance followed by Tukey's test. Food intake in non-fasted animals was much lower; it was similar in CB1<sup>+/+</sup> ( $0.19 \pm 0.05$ ,  $0.33 \pm 0.06$ ,  $0.46 \pm 0.06$  g per mouse,  $n = 8$ ) and CB1<sup>-/-</sup> mice ( $0.16 \pm 0.02$ ,  $0.33 \pm 0.04$ ,  $0.45 \pm 0.05$  g per mouse,  $n = 8$ ), at 1, 2 and 3 h, respectively.

‡ Present address: National Institute on Alcohol Abuse and Alcoholism, National Institutes of Health, MSC-8115, Bethesda, Maryland 20892-8115, USA.